International Journal of Thermophysics, Vol. 26, No. 1, January 2005 (© 2005)
DOI: 10.1007/s10765-005-2350-6

On the Interfacial Behavior about the Shield Region[1]

A. Mejía[2,3] and H. Segura[2,3]

The shield region is a singular range of the global phase diagram (GPD), where equations of state based on mean-field theories predict a quadruple point (QP) for fluid binary mixtures. The QP in question is characterized by three immiscible liquids and a vapor in equilibrium. No experimental system has been found exhibiting such an equilibrium behavior. In this theoretical study the interfacial and wetting behavior of the phases that coexist at the QP by applying the gradient theory to the van der Waals equation of state is described.

KEY WORDS: global phase diagram; interface properties; shield region; square gradient theory; quadruple point; wetting transitions.

1. INTRODUCTION

In 1968, van Konynenburg and Scott [1,2] published a seminal work regarding the capability of the van der Waals equation of state (vdW-EOS) to predict fluid phase equilibrium diagrams of binary mixtures. As a result it was found that the vdW model exhibits five main types, or classes, that differ essentially in the geometry and connectivity of the predicted critical lines. Mixtures that are classified as the same type exhibit phase diagrams of equivalent shapes and, consequently, they display similar equilibrium behavior over the whole subcritical range. A remarkable contribution of the work of van Konynenburg and Scott was the development of a

[1]Paper presented at the Fifteenth Symposium on Thermophysical Properties, June 22–27, 2003, Boulder, Colorado, U.S.A.

[2]Group of Thermodynamics. Department of Chemical Engineering, Universidad de Concepción, POB 160-C, Concepción, Chile.

[3]To whom correspondence should be addressed. E-mail: amejia@diq.udec.cl, hsegura@diq.udec.cl

map, that they called "Master Diagram" (or global phase diagram, GPD), where the prediction of each type was bounded in terms of the parameters of the vdW-EOS. Since the work of van Konynenburg and Scott, the GPD approach has been further developed, becoming a powerful tool of analysis both in theoretical and applied thermodynamics. A reduced set of GPDs have been calculated for vdW-type and theoretically based EOSs [3–11]. These studies, restricted mainly to mixtures of molecules of equal size, focus on finding all conceivable phase equilibrium behavior and result in the conclusion that all EOSs display similar GPDs. One of the most interesting phenomena found is the ability of simple models to predict four-phase equilibria inside the *shield region* [5,12] and the less known *sword region* [13].

In order to extend the systematic approach of the GPD to the case of interfacial fluids, several authors [13–24] have characterized some of the regions in terms of the thermal dependence of interface tensions and in terms of wetting transitions. From these studies, devoted mainly to two- or three-phase equilibrium, we have a better understanding on how the topological type affects the interfacial behavior.

The scope of this work is to fill some gaps regarding the interfacial behavior of mixtures that belong to the shield region (Sh-r) [12]. As pointed out before, the Sh-r is characterized by a quadruple point (QP) of equilibrium where three immiscible liquids and a gas coexist. Although no experimental binary mixture has been found exhibiting a QP of fluid phases, the results reported by Brunner [25] for water + n-alkanes mixtures (specifically when $26 < n < 28$, where an unusual tricritical transition is observed) show the trend of connectivity of the three-phase and critical lines observed in mixtures that belong to the Sh-r. In addition, a QP of fluid phases is itself interesting, since it is possible to expect a condition of high interfacial activity. In our analysis we applied the square gradient theory to vdW binary mixtures of molecules of equal size [14].

2. THEORY

2.1. Shield Region

Figure 1 depicts the Sh-r predicted by the vdW-EOS considering molecules of equal size. The coordinates of this figure are related to the parameters of the EOS according to the following definitions [1,2]:

$$\xi = \frac{b_2 - b_1}{b_2 + b_1}; \quad \zeta = \frac{a_2/b_2^2 - a_1/b_1^2}{a_2/b_2^2 + a_1/b_1^2}; \quad \lambda = \frac{a_2/b_2^2 - 2a_{12}/b_{12}^2 + a_1/b_1^2}{a_2/b_2^2 + a_1/b_1^2} \tag{1}$$

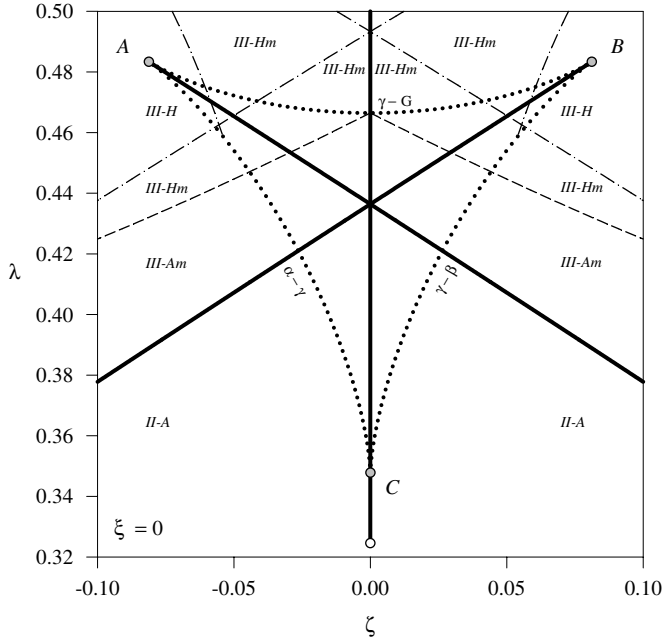

Fig. 1. Shield region for molecules of equal size, as calculated from the vdW-EOS. α, β, γ immiscible liquids, G gas phase. (—) Tricritical line, (●●●) Shield boundary, (-●-) CPSP, (– – –) III-A-H boundary.

In Eq. (1), a_i is the cohesion parameter and b_i is the covolume that, for pure vdW fluids, depend on the critical temperature T_c and critical pressure P_c according to

$$a_i = \frac{27}{64}\frac{(RT_{ci})^2}{P_{ci}}; \quad b_i = \frac{1}{8}\frac{RT_{ci}}{P_{ci}} \tag{2}$$

where R is the gas constant. In addition, the cross parameters a_{ij}, b_{ij} of Eq. (1) are given by

$$a_{12} = \sqrt{a_1 a_2}(1 - k_{12}); \quad b_{12} = \frac{b_1 + b_2}{2} \tag{3}$$

In Eq. (3), k_{12} is the interaction parameter that accounts for the magnitude and sign of the deviation of the mixture from ideal behavior.

As shown in Fig. 1, the Sh-r for mixtures of molecules of equal size ($\xi = 0$) is an almost triangular symmetric region where three tricritical boundaries, a critical-pressure step point (CPSP) boundary, and a limiting azeotropic–heteroazeotropic boundary (III-A-H line) converge. A CPSP

transition bounds the behavior of multiple pressure stationary points along a critical line in a P–T projection. In addition, the III-A-H line masks the azeotropic behavior inside a range of immiscibility. Finally, a tricritical transition breaks the continuity of a critical line in a critical end point (CEP). Due to all these transitional mechanisms, the systems that may be found inside the Sh-r are hybrids of types II and III that may present stationary pressure points and/or azeotropic behavior.

Figure 2a depicts a particular P–T projection that may be found inside the Sh-r [$\zeta = 0.04$, $\lambda = 0.46$]. Due to the previously mentioned transitional mechanisms, the general trend and connectivity of the main critical lines may vary as the ζ, λ coordinates change. However, every system drawn from the region in question exhibits QPs, as shown in Fig. 2, with the following similarities:

- the QP appears below the critical temperature of the constituents of the mixture, connecting a low-temperature three-phase line with three high-temperature three-phase lines;
- the pressure of the QP is larger than the vapor pressure of the pure components; and
- at the QP, three phases have liquid-type densities and the remaining phase has a gas-type density.

Figures 2c, d depict the phase diagrams that appear in the vicinity of the QP. It should be pointed out that the shapes of these diagrams are characteristic for every mixture inside the Sh-r. In the referenced figures it is possible to recognize a liquid phase α, rich in component *2*, and a second liquid phase β, rich in component *1*. The concentrations of the gas phase G are bounded by the concentrations of α and β. In addition, starting from the temperature of the QP, a third liquid phase γ induces a bifurcation of the low-temperature three-phase line. The liquid γ is characterized by mid-range concentrations and, depending on the coordinates of the GPD, it is able to form azeotropes.

The boundaries of the Sh-r may be calculated considering that two phases of the QP collapse in an ordinary critical point (the phases that become critical are indicated in Fig. 1). In addition, every vertex of the Sh-r corresponds to a condition where three phases of the QP collapse in a tricritical point.

In this work, we analyze the interfacial properties of the set of three-phase lines for a system with fixed ζ, λ coordinates. Then we consider the interfacial properties of the QP for single displacements in ζ and in λ, in order to analyze the influence of the components of the mixture and the synergy between components, respectively.

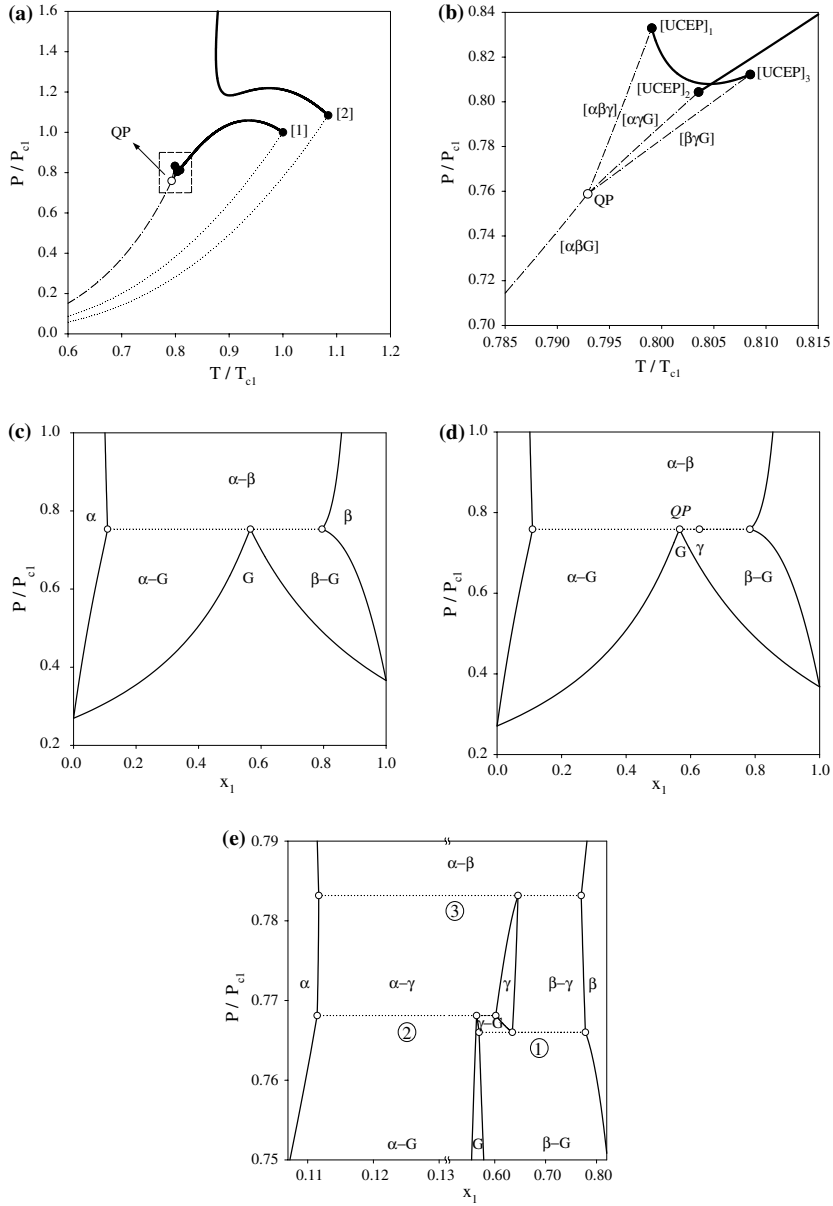

Fig. 2. (a) Pressure–temperature projection for a binary mixture at $\zeta = 0.0404$, $\lambda = 0.4550$, $\xi = 0$. (—) critical line, (• • •) vapor-pressure line, (–•–) three-phase line, (◯) QP, (•) CEPs; (b) connectivity details around the QP in Fig. 2a; (c) equilibrium diagram before the QP temperature, (◯ • • • ◯) three-phase line; (d) equilibrium diagram for the QP temperature, (◯ • • • ◯) four-phase line; and (e) equilibrium diagram after the QP temperature, (◯ • • • ◯) three-phase lines: ①$\beta\gamma G$, ②$\alpha\gamma G$, ③$\alpha\beta\gamma$.

2.2. Square Gradient Theory for Planar Interfaces

According to the gradient theory (GT) the interfacial tension (σ) between two bulk phases at equilibrium (α, β) is given by [23]

$$\sigma = \sqrt{2} \int_{\rho_s^\alpha}^{\rho_s^\beta} \sqrt{\left(a_0 - \sum_{i=1}^{n_c} \rho_i \mu_i^0 + P^0 \right) \sum_{i,j=1}^{n_c} c_{ij} \frac{d\rho_i}{d\rho_s} \frac{d\rho_j}{d\rho_s}} \, d\rho_s \tag{4}$$

In this expression, $\rho_{i,j}$ are the concentrations of species i and j and ρ_s is a reference concentration (for component i or j) whose behavior should be monotonically defined along the integral path. P^0 is the bulk equilibrium pressure, n_c stands for the number of components, a_0 is the density of the Helmholtz energy of the homogeneous system, and μ_i^0 is the chemical potential of component i at equilibrium. Both a_0 and μ_i^0 can be determined directly from any EOS [24], and c_{ij} is the cross influence parameter that is considered constant. In the present work, c_{ij} is calculated from the following expressions [23,24]:

$$\frac{c_{ii}}{a_{ii} b_{ii}^{2/3}} = \left(\frac{3}{2\pi N_{av}} \right)^{2/3}; \quad c_{ij} = \sqrt{c_{ii} c_{jj}} \tag{5}$$

where N_{av} is Avogadro's number. In Eq. (4), ρ_i and ρ_j are related by a set of partial differential equations (PDE) that describe the equilibrium condition for the interfacial fluid. However, Eq. (5) can be used to simplify the PDE problem to the following set of algebraic equations [23]:

$$\sqrt{c_{ss}} \left[\mu_k(\rho) - \mu_k^0 \right] = \sqrt{c_{kk}} \left[\mu_s(\rho) - \mu_s^0 \right] \quad k = 1, 2, \ldots, s-1, s+1, \ldots, n_c \tag{6}$$

Equation (6) allows quantification of the population of species at the interface, together with the surface activity which is characterized by the condition, $d\rho_i/d\rho_j = 0$ [23]. Physically significant solutions of Eq. (6) should be bounded by the hard-core limit of the EOS (in this case the covolume b) since at that limit, $\mu_i \to -\infty$. The numerical procedure that allows calculation of σ from Eqs. (4) and (6) was described in detail previously [24].

2.3. Wetting Transitions at Fluid Interfaces

π phases in equilibrium may be contacted by a maximum of $[1/2(\pi - 1)\pi]$ interfaces, each one of which is characterized by a specific value of σ.

For the case of three phases in equilibrium (α, β, γ), the interfacial tensions ($\sigma_{\alpha\beta}$, $\sigma_{\alpha\gamma}$, $\sigma_{\beta\gamma}$) are interrelated by [14]

$$\sigma_{\alpha\beta} < \sigma_{\alpha\gamma} + \sigma_{\beta\gamma} \quad \text{partial wetting or Neumman inequality} \tag{7a}$$

$$\sigma_{\alpha\beta} = \sigma_{\alpha\gamma} + \sigma_{\beta\gamma} \quad \text{total wetting or Antonow rule} \tag{7b}$$

The wetting condition is invariant to the cyclic permutation of the subindices α, β, γ. As written, Eqs. (7) describe the partial and total wetting of the γ phase on the $\alpha\beta$ interface. The transition from partial to total wetting (or *vice versa*) is called the w*etting transition* [14]. For the case of $\pi > 3$, no general rule exists to establish the mathematical condition of a wetting transition. Intuitively, it is possible to infer that a basic condition for a wetting transition is that, at the least, every set of $(\pi - 1)$ phases should be at the wetting transition. Following this argument, we can expect that a wetting transition at the QP ($\pi = 4$) requires a wetting transition condition for every set of three phases that we could select from the QP. Following such an hypothesis, the wetting transitions of a QP may be analyzed using Eqs. (7).

3. RESULTS AND DISCUSSION

3.1. Interface Behavior at Fixed ζ, λ Coordinates

The objective of this section is to analyze the ρ–ρ and σ–T projections for the QP of a specific mixture inside the Sh-r, and to illustrate the connectivity of its interfacial tensions. The GPD coordinates, critical properties, and interaction parameter of the mixture are indicated in Table I. Figure 2 illustrates the critical P–T projection and the phase diagrams for the system in question. The thermal evolution of the ρ–ρ projections for each three-phase line that meets the QP is shown in Fig. 3. From these figures we can conclude that the Sh-r exhibits dominant surface activity, as follows from the stationary condition $d\rho_i/d\rho_j = 0$. Inspection of Fig. 3 reveals that the ρ–ρ projections of every three-phase line converge to a single trajectory at the QP, whose ρ–ρ projection is shown in Fig. 4. Figures 5 and 6 show the σ–T projections for the complete set

Table I. GDP Coordinates, Critical Properties, and Interaction Parameter for the Mixture in Fig. 2

ζ	λ	T_{c2}/T_{c1}	P_{c2}/P_{c1}	k_{12}
0.0404	0.4550	1.084109	1.084109	0.454556

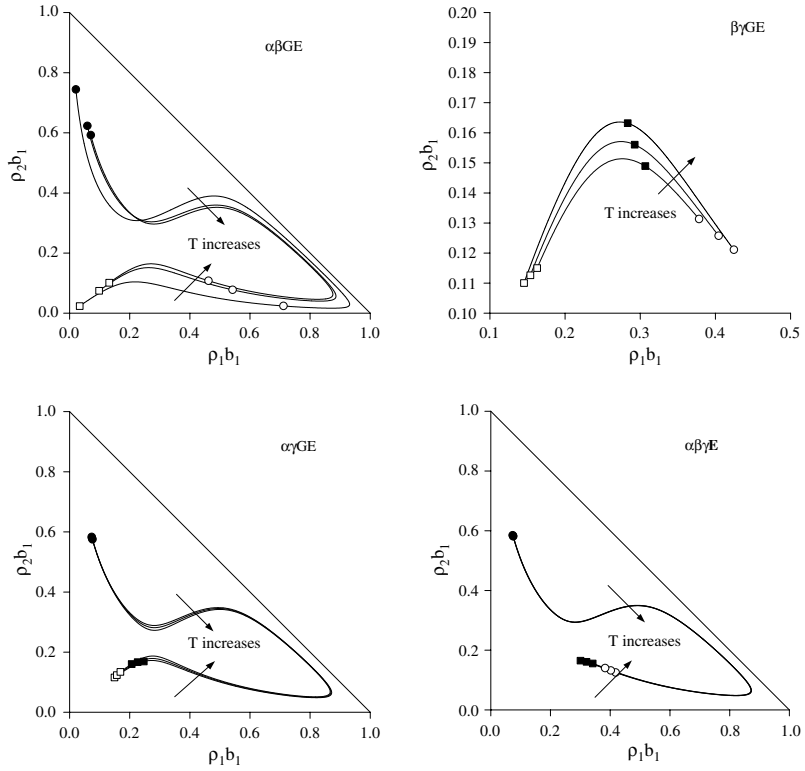

Fig. 3. Thermal evolution of interfacial concentrations for three-phase lines. (●) α bulk phase, (○) β bulk phase, (■) γ bulk phase, (□) G bulk phase.

of three-phase lines that connect the QP. The interfacial behavior of the mixture under analysis is summarized in Tables II and III. From these results, we can conclude that the interfacial tensions along the three-phase lines exhibit the usual trend that can be expected for heteroazeotropes at subcritical and critical conditions, as we described previously [24].

Focusing our attention on the QP, we can observe that the interfacial tensions of the low temperature three-phase line connect the interfacial tensions of the high temperature three-phase lines for the $\alpha\beta$, αG, and βG interfaces. It is clear also that the temperature slope of these interfacial tensions change at the QP. In addition, due to the generation of the γ phase, additional interfacial tensions related to the γ interface appear at $T \geqslant T_{\mathrm{QP}}$. In fact the QP is characterized by *six interfacial* tensions of different orders of magnitude.

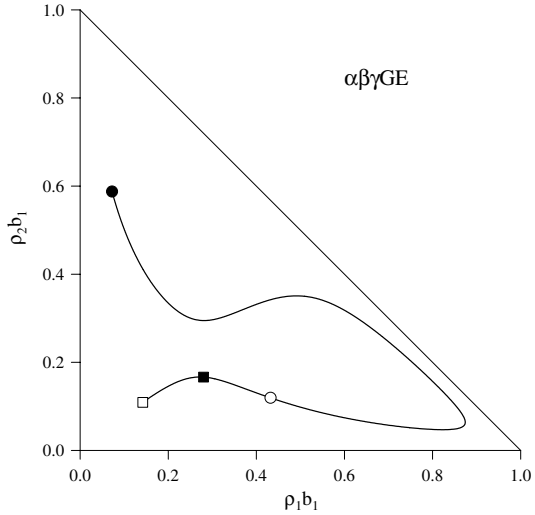

Fig. 4. Interfacial concentrations at the QP. (●) α bulk phase, (◯) β bulk phase, (■) γ bulk phase, (□) G bulk phase.

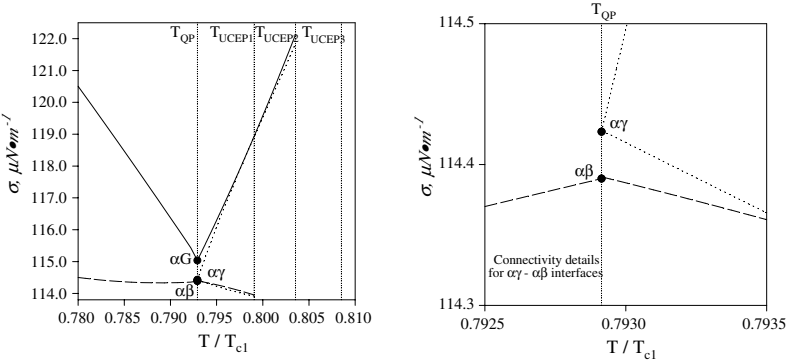

Fig. 5. Thermal evolution of interfacial tension around the QP. Region of high interfacial tensions. (—) $\sigma_{\alpha G}$, (- - -) $\sigma_{\alpha\beta}$, (●●●) $\sigma_{\alpha\gamma}$, (●) σ at QP.

3.2. Interface Behavior for the QP along the λ Coordinate

The objective of this section is to describe the impact of the λ coordinate on the interface behavior. A constant ζ value implies that the critical properties of a mixture do not vary as λ changes. Consequently, from Eqs. (1), it follows that single λ displacements are related to variations of

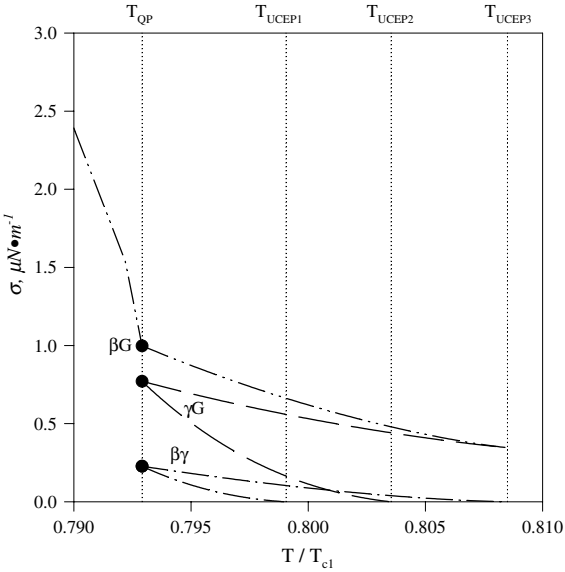

Fig. 6. Thermal evolution of interfacial tension around the QP. Region of low interfacial tensions. (–•–) $\sigma_{\beta\gamma}$, (–•–) $\sigma_{\beta G}$, (— —) $\sigma_{\gamma G}$, (●) σ at QP.

k_{12}. Consequently, this analysis reflects the influence of the synergy of the mixture on the interfacial properties of the QP.

Figure 7 depicts the evolution of the ρ–ρ projection as λ increases. Minor variations could be observed, allowing the deduction that the surface activity of the interface does not vary significantly with λ.

Figure 8 illustrates the evolution of the six interfacial tensions of the QP. We can observe that, as λ increases, four interfacial tensions increase ($\sigma_{\alpha G}$, $\sigma_{\alpha\gamma}$, $\sigma_{\alpha\beta}$, $\sigma_{\beta\gamma}$) and two decrease ($\sigma_{\beta G}$, $\sigma_{\gamma G}$). In addition, these figures show that the interfacial behavior is in agreement with the critical collapse of the γG and the $\alpha\gamma$ phases at the upper and lower limits of the Sh-r (see Fig. 1). General results have been summarized in Table IV.

Similar results can be found for every $\zeta \in (0; 0.0507]$. As a consequence of the symmetry of the GPD for molecules of equal size, the range $\zeta \in [-0.0507; 0)$ exhibits the same patterns described before. Finally, analyzing the $\sigma(\lambda)$ curves and considering Eqs. (7), we can conclude that, for the analyzed ranges, no wetting transitions are observed for the four phases of the QP.

Table II. Interfacial Tension Behavior along the Three-Phase Lines of Fig. 2

Temperature range	Phase equilibrium condition	Interfacial tension behavior
$\alpha\beta G$E-line		
$T < T_{QP}$	Subcritical equilibrium	$\sigma_{\alpha G} \neq \sigma_{\beta G} \neq \sigma_{\alpha\beta} \neq 0$
	$\alpha G,\ \beta G$	σ decreases as T increases
	$\alpha\beta$	σ exhibits stationary points in T
$T = T_{QP}$	Subcritical equilibrium	$\sigma_{\alpha G} \neq \sigma_{\beta G} \neq \sigma_{\alpha\beta} \neq 0$
	$\alpha G, \beta G, \alpha\beta$	
$\alpha\beta\gamma$ E-line		
$T = T_{QP}$	Subcritical equilibrium	$\sigma_{\alpha\beta} \neq \sigma_{\alpha\gamma} \neq \sigma_{\beta\gamma} \neq 0$
	$\alpha\beta, \alpha\gamma, \beta\gamma$	
$T_{QP} < T < T_{UCEP1}$	Subcritical equilibrium	$\sigma_{\alpha\beta} \neq \sigma_{\alpha\gamma} \neq \sigma_{\beta\gamma} \neq 0$
	$\alpha\gamma,\ \beta\gamma$	σ decreases as T increases
	$\alpha\beta$	σ exhibits stationary points in T
$T = T_{UCEP1}$	Subcritical equilibrium	$\sigma_{\alpha\beta} \neq \sigma_{\alpha\gamma} \neq 0$
	$\alpha\beta,\ \alpha\gamma$	
	Critical equilibrium	$\sigma_{\beta\gamma} = 0$
	$\beta\gamma$	
$\alpha\gamma G$E-line		
$T = T_{QP}$	Subcritical equilibrium	$\sigma_{\alpha\gamma} \neq \sigma_{\alpha_G} \neq \sigma_{\gamma G} \neq 0$
	$\alpha\gamma,\ \alpha G,\ \gamma G$	
$T_{QP} < T < T_{UCEP2}$	Subcritical equilibrium	$\sigma_{\alpha\gamma} \neq \sigma_{\alpha G} \neq \sigma_{\gamma G} \neq 0$
	$\alpha G,\ \gamma G$	σ increases as T increases
	$\alpha\gamma$	σ decreases as T increases
$T = T_{UCEP2}$	Subcritical equilibrium	$\sigma_{\alpha G} \neq \sigma_{\gamma G} \neq 0$
	$\alpha G, \gamma G$	
	Critical equilibrium	$\sigma_{\alpha\gamma} = 0$
	$\alpha\gamma$	
$\beta\gamma G$E-line		
$T = T_{QP}$	Subcritical equilibrium	$\sigma_{\gamma\beta} \neq \sigma_{\gamma G} \neq \sigma_{\beta G} \neq 0$
	$\gamma\beta, \gamma G, \beta G$	
$T_{QP} < T < T_{UCEP3}$	Subcritical equilibrium	$\sigma_{\alpha G} \neq \sigma_{\beta G} \neq \sigma_{\alpha\beta} \neq 0$
	$\gamma\beta,\ \gamma G,\ \beta G$	σ decreases as T increases
$T = T_{UCEP3}$	Subcritical equilibrium	$\sigma_{\beta G} = \sigma_{\gamma_G} \neq 0$
	$\beta G = \gamma G$	
	Critical equilibrium	$\sigma_{\beta\gamma} = 0$
	$\beta\gamma$	

3.3. Interface Behavior for the QP along the ζ Coordinate

The objective of this section is to analyze the ρ–ρ and σ–ζ projections of the QP as ζ varies with constant λ. Such an incursion reflects the influence of the critical properties of the constituents of a mixture. Figure 9 shows the ρ–ρ projections for the different values that ζ may

Table III. Wetting Behavior along the Three-Phase Lines of Fig. 2

Temperature range	Wetting behavior	Wetting regime
$\alpha\beta GE$-line		
$T \leq T_{QP}$	$\sigma_{\alpha\beta} < \sigma_{\alpha G} + \sigma_{\beta G}$ $\sigma_{\alpha G} < \sigma_{\alpha\beta} + \sigma_{\beta G}$ $\sigma_{\beta G} < \sigma_{\alpha\beta} + \sigma_{\alpha G}$	No wetting transition
$\alpha\beta\gamma GE$-line		
$T_Q < T < T_{UCEP1}$	$\sigma_{\alpha\gamma} < \sigma_{\alpha\beta} + \sigma_{\gamma\beta}$ $\sigma_{\gamma\beta} < \sigma_{\alpha\gamma} + \sigma_{\alpha\beta}$	No wetting transition
$T_{QP} < T < T_w$	$\sigma_{\alpha\beta} < \sigma_{\alpha\gamma} + \sigma_{\gamma\beta}$	No wetting transition
$T = T_w$	$\sigma_{\alpha\beta} = \sigma_{\alpha\gamma} + \sigma_{\gamma\beta}$	Wetting transition at $T_w = 0.7961$
$T_w < T < T_{UCEP1}$	$\sigma_{\alpha\beta} > \sigma_{\alpha\gamma} + \sigma_{\gamma\beta}$	No wetting transition
$\alpha\gamma GE$-line		
$T_{QP} < T < T_{UCEP2}$	$\sigma_{\alpha\gamma} < \sigma_{\alpha G} + \sigma_{\gamma G}$ $\sigma_{\gamma G} < \sigma_{\alpha\gamma} + \sigma_{\alpha G}$	No wetting transition
$T_{QP} < T < T_w$	$\sigma_{\alpha G} < \sigma_{\alpha\gamma} + \sigma_{\gamma G}$	No wetting transition
$T = T_w$	$\sigma_{\alpha G} = \sigma_{\alpha\gamma} + \sigma_{\gamma G}$	Wetting transition at $T_w = 0.8007$
$T_w < T < T_{UCEP2}$	$\sigma_{\alpha G} > \sigma_{\alpha\gamma} + \sigma_{\gamma G}$	No wetting transition
$\beta\gamma GE$-line		
$T_{QP} < T < T_{UCEP3}$	$\sigma_{\alpha\beta} < \sigma_{\alpha G} + \sigma_{\beta G}$ $\sigma_{\alpha G} < \sigma_{\alpha\beta} + \sigma_{\beta G}$ $\sigma_{\beta G} < \sigma_{\alpha\beta} + \sigma_{\alpha G}$	No wetting transition

acquire inside the Sh-r. From this figure it is possible to conclude that variations on the ζ coordinate strongly affect the surface activity. Such a behavior follows from the fact that ζ variations change the c_{ij} values and, therefore, the interfacial tensions of the pure components.

In Fig. 9 we can also see that, at $\zeta = 0$, the solution of Eqs. (6) tends to the limit $\mu_i \to -\infty$ (such a condition appears along the asymptotic segment BC). In addition, the ρ–ρ projection becomes a nondifferentiable function at point A, where the mixture is composed of equivalent molecules with large synergy. As may be deduced from Eq. (4), the nondifferentiable point corresponds to a condition that affects the prediction of σ. It is clear that point A implies a shape transition point (ST_p) on density profiles and yields a singularity for the $d\rho_1/d\rho_2$ derivative.

Figure 10 depicts the dependence of σ for the whole range of ζ. As was discussed previously for Figs. 4 and 8, the QP is characterized again by high and low interface tensions. In addition, we can observe that, at the ST_p, the subset of interfacial tensions that do not include the γ–G interface are not continuous on ζ.

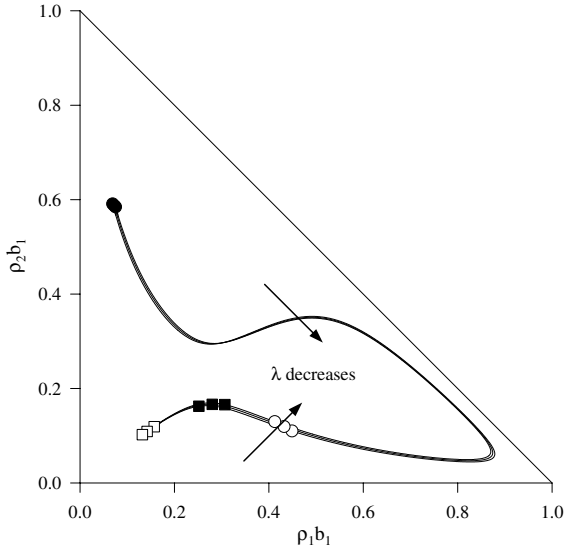

Fig. 7. Dependence of interfacial concentrations on $\lambda(\zeta = 0.0404, \xi = 0)$. (●) α bulk phase, (◯) β bulk phase, (■) γ bulk phase, (□) G bulk phase, λ values are: 0.4485, 0.4550, 0.4624.

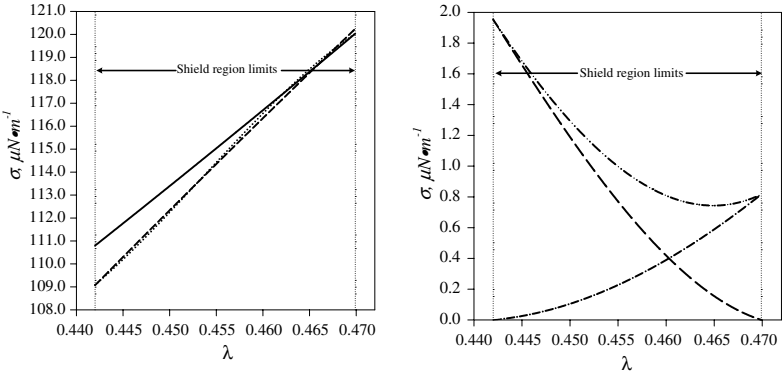

Fig. 8. Dependence of interfacial tensions on λ ($\zeta = 0.0404, \xi = 0$). (—) $\sigma_{\alpha G}$, (- - -) $\sigma_{\alpha\beta}$, (●●●) $\sigma_{\alpha\gamma}$, (–●–) $\sigma_{\beta\gamma}$, (–●●–) $\sigma_{\beta G}$, (— —) $\sigma_{\gamma G}$.

It should be pointed out that the ST_p coincides with the symmetric tricritical line observed in Fig. 1; however, the ST_p is not necessarily associated with a tricritical transition. In fact, Fig. 11a illustrates the Sh-r for molecules of different sizes ($\xi = -0.23$). From the figure in question,

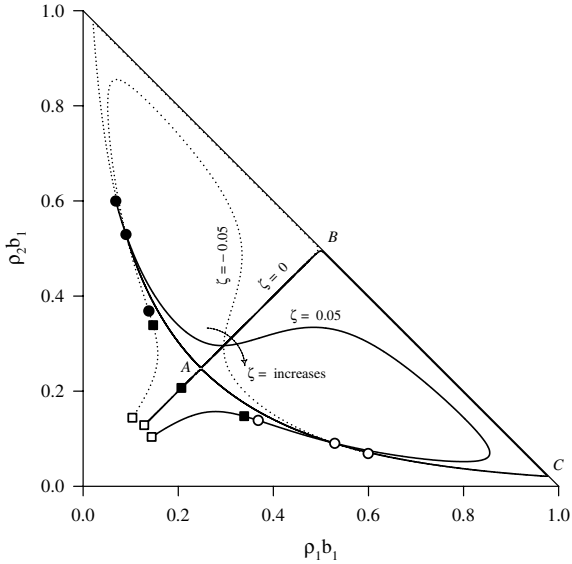

Fig. 9. Dependence of interfacial concentrations on $\zeta(\lambda = 0.4550, \xi = 0)$. (●) α bulk phase, (○) β bulk phase, (■) γ bulk phase, (□) G bulk phase.

we can observe an ST_p line on the GPD (line CD), that goes from the lower tricritical vertex C to a nontricritical upper point D of the Sh-r. Figure 11b shows the pertinent QP σ values that may be calculated for the whole ζ range at $\lambda = 0.4770$. As in the case of mixtures of molecules of equal size, every interfacial tension not related to the γ–G interface becomes evidently disconnected at the ST_p, yielding thus an undefined wetting behavior.

4. CONCLUDING REMARKS

In this work we have analyzed interface properties and wetting transitions for mixtures that belong to the shield region. Special attention has been given to the properties of the QP, which is the common characteristic of the mixtures under analysis. Calculations have been based on the GT applied to the vdW-EOS. The main advantage of this approach is that calculations are based on the same EOS, yielding thus a coherent theory for relating equilibrium features with interface properties. According to results, the shield region is characterized by a shape transition point of density profiles, around which similar ρ–ρ projections and strong

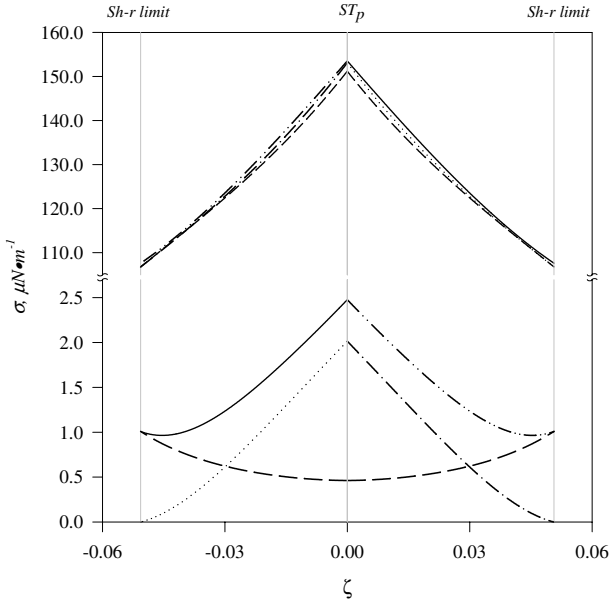

Fig. 10. Dependence of interfacial tensions on $\zeta(\lambda = 0.4550, \xi = 0)$. (—) Sh-r limits, (—) shape transition line, (—) $\sigma_{\alpha G}$, (- - -) $\sigma_{\alpha\beta}$, (●●●) $\sigma_{\alpha\gamma}$, (–●–) $\sigma_{\beta\gamma}$, (–●●–) $\sigma_{\beta G}$, (— —) $\sigma_{\gamma G}$.

surface activity are predicted. The QPs of the shield region are characterized by six interfacial tensions of different orders of magnitude, whose continuity on ζ becomes undefined at the density profile shape Ptransition point. The discontinuity of interfacial tensions implies also an undefined local wetting regime. In addition, ρ–ρ projections are very sensitive to changes in the ζ coordinate, due to variation of the influence parameter c_{ij}, and less sensitive to the λ coordinate. It follows then that the interfacial properties of the shield region exhibit a strong dependence on the components of the mixture and a weaker dependence on its synergy.

Inside the range of conditions analyzed in this work, no wetting transition involves the four phases of the QP.

ACKNOWLEDGMENT

This work was financed by FONDECYT, Santiago, Chile (Projects 1020340 and 2010100).

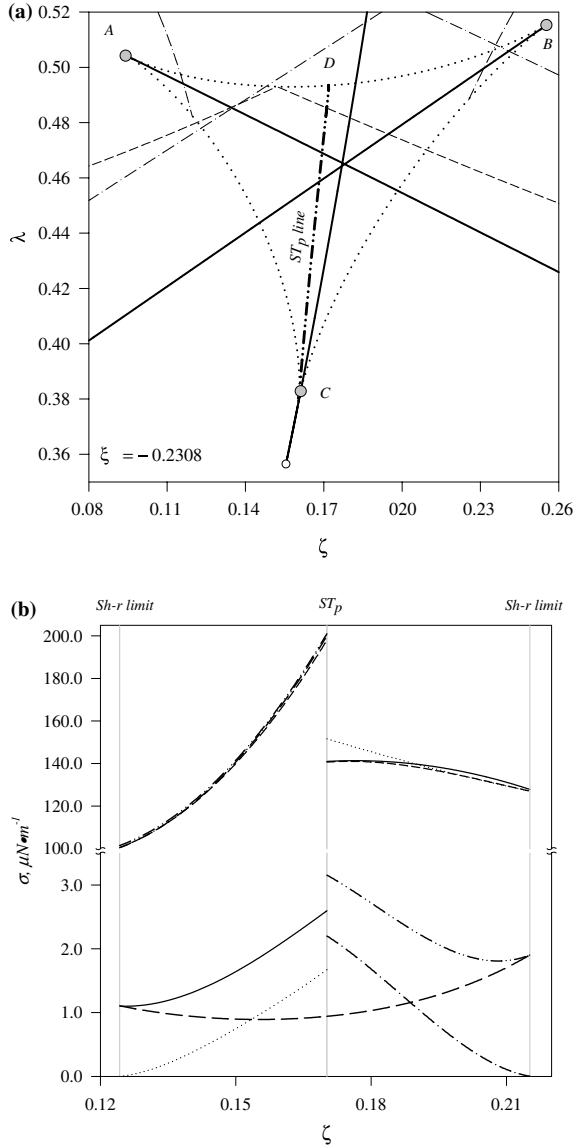

Fig. 11. (a) Shield region for molecules of different size ($\xi = -0.2308$), as calculated from the vdW-EOS, (–••–) shape transition line, remaining captions as in Fig. 1; (b) dependence of interfacial tensions on ζ ($\lambda = 0.4770, \xi = -0.2309$). (—) Sh-r limits, (—) shape transition line, (—) $\sigma_{\alpha G}$, (- - -) $\sigma_{\alpha\beta}$, (•••) $\sigma_{\alpha\gamma}$, (–•–) $\sigma_{\beta\gamma}$, (–••–) $\sigma_{\beta G}$, (— —) $\sigma_{\gamma G}$.

REFERENCES

1. P. van Konynenburg, *Critical Lines and Phase Equilibria in Binary van der Waals Mixtures* (Ph.D. Thesis, University of California, 1968).
2. P. van Konynenburg and R. Scott, *Philos. Trans. R. Soc. London, Ser A* **298**:495 (1980).
3. D. Furman, S. Dattagupta, and R. B. Griffiths, *Phys. Rev. B.* **15**:441 (1977).
4. L. Z. Boshkov and V. A. Mazur, *Russ. J. Phys. Chem*. **60**:16 (1986).
5. I. C. Wei and R. L. Scott, *J. Stat. Phys*. **52**:1315 (1988).
6. P. H. E. Meijer, O. L. Pegg, J. Aronson, and M. Keskin, *Fluid Phase Equilib*. **58**:65 (1990).
7. L. Z. Boshkov and L. V. Yelash, *Fluid Phase Equilib*. **141**:105 (1997).
8. L. Z. Boshkov and L. V. Yelash, *Doklady Akademii Nauk*. **341**:61 (1995).
9. U. K. Deiters and I. L. Pegg, *J. Chem. Phys*. **90**:6632 (1989).
10. T. Kraska and U. K. Deiters, *J. Chem. Phys*. **96**:539 (1991).
11. T. Kraska. *Ber. Bunsenges. Phys. Chem*. **100**:1318 (1996).
12. D. Furman and R. B. Griffiths, *Phys. Rev. A.* **17**:1139 (1978).
13. U. K. Deiters, L. Z. Boshkov, L. V. Yelash, and V. A. Mazur, *Doklady Akademii Nauk.* **359**:343 (1998).
14. J. S. Rowlinson and B. Widom, *Molecular Theory of Capillarity* (Oxford University Press, Oxford, 1982).
15. D. E. Sullivan, *J. Chem. Phys*. **77**:2632 (1982).
16. M. E.Costas, C. Vera, and A. Robledo, *Phys. Rew. Lett*. **51**:2394 (1983).
17. P. M. W. Cornelisse, *The Gradient Theory Applied, Simultaneous Modelling of Interfacial Tension and Phase Behaviour* (Ph.D. Thesis, Delft University, 1997).
18. I. A. McLure, R. Whitfield, and J. Bowers, *J. Colloid Interface Sci*. **203**:31 (1998).
19. C. Pérez, P. Roquero, and V. Talanquer, *J. Chem. Phys*. **100**:5913 (1994).
20. M. M. Telo da Gama and R. Evans, *Mol. Phys*. **48**:229 (1983).
21. M. M. Telo da Gama and R. Evans, *Mol. Phys*. **48**:251 (1983).
22. P. Tarazona, M. M. Telo da Gama, and R. Evans, *Mol. Phys*. **49**:283 (1983).
23. B. S. Carey, *The GradientTheory of Fluid Interfaces* (Ph.D. Thesis, University of Minnesota, 1979).
24. A. Mejía and H. Segura. *Int. J. Thermophys*. **25**: 1395 (2004).
25. E. Brunner, *J. Chem. Thermodynamics*. **22**:335 (1990).